Article

Cell

Glucose Uptake and Runx2 Synergize to Orchestrate Osteoblast Differentiation and Bone Formation

Graphical Abstract

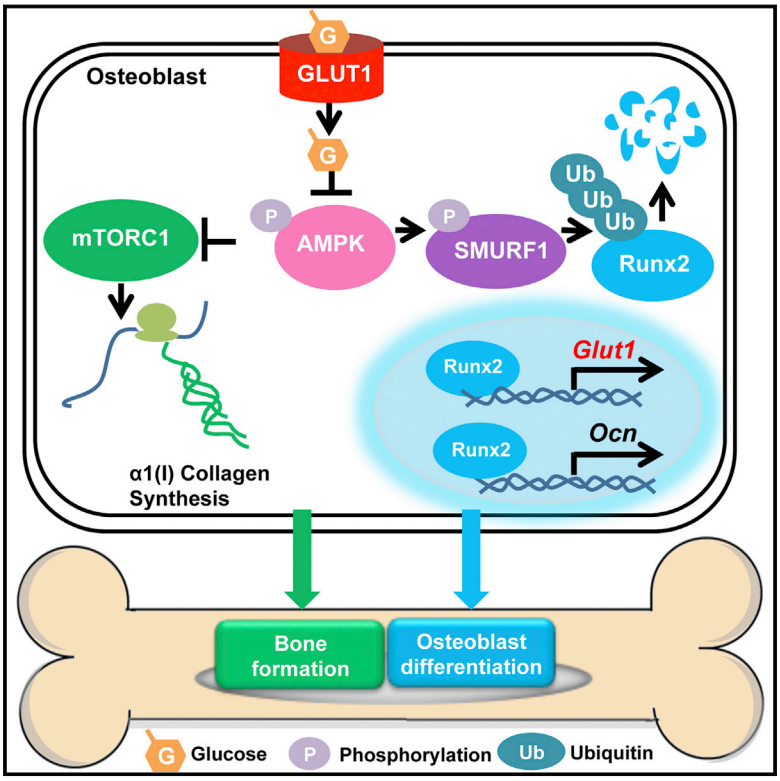

Highlights

- Osteoblasts are addicted to glucose
- Glucose uptake is needed for osteoblast differentiation and bone formation
- Runx2 is necessary for Glut1 expression in prospective osteoblasts
- Glut1 and Runx2 crosstalk determines osteoblast differentiation and bone formation

Authors

Jianwen Wei, Junko Shimazu, Munevver P. Makinistoglu, ..., Jeffrey E. Pessin, Eiichi Hinoi, Gerard Karsenty

Correspondence

gk2172@cumc.columbia.edu

In Brief

Osteoblasts paradoxically secrete the main constituent of the bone matrix before turning on their master differentiation gene *Runx2*. These cells are addicted to glucose, whose uptake coordinates osteoblast differentiation and bone formation through crosstalk with *Runx2*, revealing a key regulatory role for metabolic demand.

Wei et al., 2015, Cell *161*, 1576–1591
June 18, 2015
http://dx.doi.org/10.1016/j.cell.2015.05.029

CellPress

Cell

Article

Glucose Uptake and Runx2 Synergize to Orchestrate Osteoblast Differentiation and Bone Formation

Jianwen Wei,[1,4] Junko Shimazu,[1,4] Munevver P. Makinistoglu,[1] Antonio Maurizi,[1] Daisuke Kajimura,[1] Haihong Zong,[2] Takeshi Takarada,[3] Takashi Iezaki,[3] Jeffrey E. Pessin,[2] Eiichi Hinoi,[3] and Gerard Karsenty[1,*]

[1]Department of Genetics and Development, College of Physicians and Surgeons, Columbia University, New York, NY 10032, USA
[2]Department of Medicine and Molecular Pharmacology, The Albert Einstein College of Medicine, Bronx, New York, NY 10461, USA
[3]Faculty of Pharmacy, Laboratory of Molecular Pharmacology, Institute of Medical, Pharmaceutical, and Health Sciences, Kanazawa University, Kanazawa, Ishikawa 920-1192, Japan
[4]Co-first author
*Correspondence: gk2172@cumc.columbia.edu
http://dx.doi.org/10.1016/j.cell.2015.05.029

SUMMARY

The synthesis of type I collagen, the main component of bone matrix, precedes the expression of *Runx2*, the earliest determinant of osteoblast differentiation. We hypothesized that the energetic needs of osteoblasts might explain this apparent paradox. We show here that glucose, the main nutrient of osteoblasts, is transported in these cells through *Glut1*, whose expression precedes that of *Runx2*. Glucose uptake favors osteoblast differentiation by suppressing the AMPK-dependent proteasomal degradation of Runx2 and promotes bone formation by inhibiting another function of AMPK. While RUNX2 cannot induce osteoblast differentiation when glucose uptake is compromised, raising blood glucose levels restores collagen synthesis in *Runx2*-null osteoblasts and initiates bone formation in *Runx2*-deficient embryos. Moreover, RUNX2 favors *Glut1* expression, and this feedforward regulation between RUNX2 and *Glut1* determines the onset of osteoblast differentiation during development and the extent of bone formation throughout life. These results reveal an unexpected intricacy between bone and glucose metabolism.

INTRODUCTION

The transcription factor RUNX2 is a master determinant of osteoblast differentiation (Long, 2012; Karsenty et al., 2009). Its expression in prospective osteoblasts precedes osteoblast differentiation; its inactivation prevents osteoblast differentiation; and its haplo-insufficiency causes a skeletal dysplasia called cleidocranial dysplasia (CCD), which is characterized by a delay in osteoblast differentiation, leading to hypoplastic clavicles and open fontanelles. Several aspects of Runx2 biology, however, remain poorly understood. For example, the nature of the molecular events leading to RUNX2 accumulation in cells of the osteoblast lineage is largely unknown. Another question is to determine if and how RUNX2 contributes to bone formation by differentiated osteoblasts. A peculiar feature of osteoblast biology raises this latter issue.

Type I collagen is by far the most abundant protein of bone extracellular matrix (ECM), and its synthesis by osteoblasts is often considered a biomarker of bone formation. Type I collagen is a heterotrimeric protein made of two α1(I) chains and one α2(I) chain, which are encoded by two different genes (Vuorio and de Crombrugghe, 1990). In vitro, RUNX2 can bind to and upregulate the activity of an *α1(I) Collagen* promoter fragment (Kern et al., 2001). However, in vivo type I collagen synthesis precedes *Runx2* expression in prospective osteoblasts. Thus, the regulation of type I collagen synthesis in osteoblasts is not fully understood, and by extension, since bone ECM is mainly made of type I collagen, it is also unclear how bone formation by osteoblasts is regulated.

Besides being responsible for bone formation, osteoblasts are endocrine cells that secrete the hormone osteocalcin, which favors glucose homeostasis (Lee et al., 2007). Notwithstanding the molecular complexity of this emerging regulation, the identification of bone as a regulator of glucose metabolism raises a fundamental question: why would bone have this role? A prerequisite to answering this question is to define the functions of glucose in osteoblasts.

Here, we asked if the energetic needs of the osteoblast might explain how osteoblast differentiation and bone formation occurs in vivo. We found that glucose is the main nutrient of osteoblasts and it is transported in these cells in an insulin-independent manner through the facilitative *Glut1* glucose transporter whose expression precedes that of *Runx2* during skeletogenesis. By inhibiting one activity of AMPK, glucose is necessary for RUNX2 accumulation and osteoblast differentiation; through the inhibition of another AMPK function, glucose is necessary for collagen synthesis and bone formation. Moreover, by promoting RUNX2 accumulation, glucose uptake in osteoblasts favors *Osteocalcin* expression and whole-body glucose homeostasis. We further show that RUNX2 is not sufficient for timely osteoblast differentiation and proper bone formation if glucose uptake is compromised, whereas raising blood glucose levels induces collagen synthesis and bone formation in the absence of *Runx2*. The relationship between RUNX2 and glucose uptake is even more

elaborate since RUNX2 is needed for *Glut1* expression in osteoblasts. This crosstalk between RUNX2 and glucose uptake acts as an amplification mechanism, allowing osteoblast differentiation and bone formation to be coordinated throughout life. This study provides a bone-centric illustration of the importance of crosstalk between bone and glucose metabolism.

RESULTS

Insulin-Independent Glucose Uptake in Osteoblasts

To determine the main nutrient(s) used by osteoblasts, we measured the oxygen consumption rate (OCR) of osteoblasts when incubated with individual nutrients. Like neurons and unlike myoblasts, osteoblasts had the highest OCR when cultured in the presence of glucose and the lowest when cultured in the presence of a representative fatty acid (Figure 1A). These results prompted us to measure, through euglycemic hyperinsulinemic clamps, the amount of glucose taken up by bone and the mechanism by which it occurs in 3-month-old wild-type (WT) mice.

In the conditions of this assay, bone takes up one-fifth of the quantity of glucose taken up by skeletal muscle, the tissue taking up the majority of glucose in the mouse (Ferrannini et al., 1988), and one-half of what is taken up by white adipose tissue (WAT) (Figure 1B). Unlike uptake for skeletal muscle and WAT, glucose uptake in bone is not enhanced by insulin (Figure 1B). We also compared the uptake of 2-[U-^{14}C] deoxyglucose (2-DG) in osteoblasts and osteoclasts to that in myoblasts. Both bone cell types take up approximately one-third of the quantity of 2-DG taken up by myoblasts and do so in an insulin-independent manner (Figure 1C). Consistent with these observations, *Glut1*, which transports glucose in an insulin-independent manner, is expressed two orders of magnitude higher than any other class I glucose transporter in bone cells (Figure 1D). The rest of this study focuses on the functions of glucose in osteoblasts.

To establish the biological importance of *Glut1* expression in these cells, we analyzed osteoblasts lacking or overexpressing modestly (1.75-fold) *Glut1* (Figures S1A and S1B). *Glut1*−/− osteoblasts took up 75% less 2-DG, and *α1(I)Col-Glut1* osteoblasts took up 20% more 2-DG than did control osteoblasts (Figure 1E). Consequently, glycogen content was decreased 50% in *Glut1*−/− and increased 40% in *α1(I)Col-Glut1* osteoblasts compared to controls (Figure S1C). Thus, GLUT1 is responsible for the majority of glucose uptake in osteoblasts.

Glucose Uptake Is Necessary for Osteoblast Differentiation during Development

Next, we analyzed the spatial and temporal pattern of *Glut1* expression during skeletogenesis by in situ hybridization and compared it to that of *α1(I) Collagen* and *Runx2*, two marker genes of mesenchymal cells and osteoblasts, of *α1(II) Collagen*, a marker of non-hypertrophic chondrocytes, and of *α1(X) collagen*, a marker of hypertrophic chondrocytes.

At E10.5 *Glut1* is highly expressed in *α1(I) Collagen*-expressing mesenchymal cells of the developing hindlimbs (Figures 1Fa–1Fj). *Runx2* is expressed in *α1(I) Collagen/Glut1*-expressing cells at E12.5 and is expressed in these cells throughout development (Figures 1Fk–1Fo). Prior to E12.5, another *Runx* gene, *Runx1*, is expressed in *α1(I) Collagen/Glut1*-expressing cells (Figures 1Fp–1Ft). The third *Runx* gene, *Runx3*, is not expressed before E13.5, and its expression is predominant in *α1(II) Collagen*-expressing chondrocytes (Figures 1Fu–1Fy and 1Fz–1Fb1). *Glut1* is virtually not expressed in chondrocytes (Figures 1Fa–1Fe and 1Fz–1Fe1). In view of this pattern of expression, we analyzed the function of *Glut1* during osteoblast differentiation by crossing mice harboring a floxed allele of *Glut1* (Figure S2A) with mice expressing the *Cre* recombinase under the control of *Dermo1* (Yu et al., 2003) (*Glut1*$_{dermo1}$−/−), which deletes genes starting at E12.5, or of *Osterix* regulatory elements (Rodda and McMahon, 2006) (*Glut1*$_{osx}$−/−), which deletes genes starting at E14.5. We verified in each case that *Glut1* was efficiently deleted in the targeted cells, but not in other cell types or tissues, and that expression of other *Gluts* was not affected by the *Glut1* deletion (Figures S2B–S2E).

Using alcian blue/alizarin red staining of skeletal preparations to distinguish non-mineralized (blue) from mineralized ECM (red), *Glut1*$_{dermo1}$−/− and control embryos were indistinguishable until E13.5 (Figure S2F). E14.0 was the first time point at which a delay in ECM mineralization in long bones and the jaws was seen in *Glut1*$_{dermo1}$−/− embryos (Figure 2A). This difference in ECM mineralization between control and *Glut1*$_{dermo1}$−/− embryos was verified histologically (Figure 2B). At E14.5, ECM mineralization was still absent in the mandibles of *Glut1*$_{dermo1}$−/− embryos (Figure 2A). Beyond E14.5, we also studied *Glut1*$_{osx}$−/− embryos. At E15.5, a large area of mineralized ECM was present in the axial skeleton of controls, but not in that of *Glut1*$_{osx}$−/− and *Glut1*$_{dermo1}$−/− embryos, except in long bones (Figures 2C and S2F). Von Kossa staining of histological sections detected extensive ECM mineralization in skeletal elements of control embryos, while this mineralization was more restricted in *Glut1*$_{osx}$−/− embryos; alcian blue staining of these sections showed that ECM in *Glut1*$_{osx}$−/− skeletal elements was mostly of cartilaginous nature (Figure 2D). Consistent with this observation, *α1(X) Collagen*-expressing hypertrophic chondrocytes covered a larger area in *Glut1*$_{osx}$−/− than in control skeletal elements, and expression of *Osteocalcin* was undetectable in *Glut1*$_{osx}$−/− skeletal elements (Figure 2E), indicating that osteoblast differentiation was delayed in E15.5 *Glut1*$_{osx}$−/− embryos. Remarkably, despite these delays in osteoblast differentiation and bone formation, *Runx2* and *α1(I) Collagen* were normally expressed in E15.5 *Glut1*$_{osx}$−/− skeletal elements (Figure 2E).

At E18.5, *Glut1*$_{osx}$−/− embryos' skulls, which ossify mostly through an intramembranous process, were poorly mineralized, suggesting that osteoblast differentiation was delayed (Figure 2F). Von Kossa staining of histological sections showed numerous long, thick trabeculae in controls, but not in *Glut1*$_{osx}$−/−, long bones, and an alcian blue staining showed many more cartilaginous remnants in *Glut1*$_{osx}$−/− than in control skeletal elements (Figure 2G). Accordingly, the area occupied by *α1(X) Collagen*-expressing hypertrophic chondrocytes remained larger in *Glut1*$_{osx}$−/− than in control skeletal elements, and expression of *Osteocalcin* was still barely detectable (Figures 2H–2J). This incomplete osteoblast differentiation in *Glut1*$_{osx}$−/− bones and osteoblasts was further illustrated by the decreased expression of *Bsp* (Figures 2I and 2J). This delay in osteoblast differentiation explains why E18.5 *Glut1*$_{osx}$−/− embryos had open fontanelles and hypoplastic clavicles (Figure 2F). Even though these two

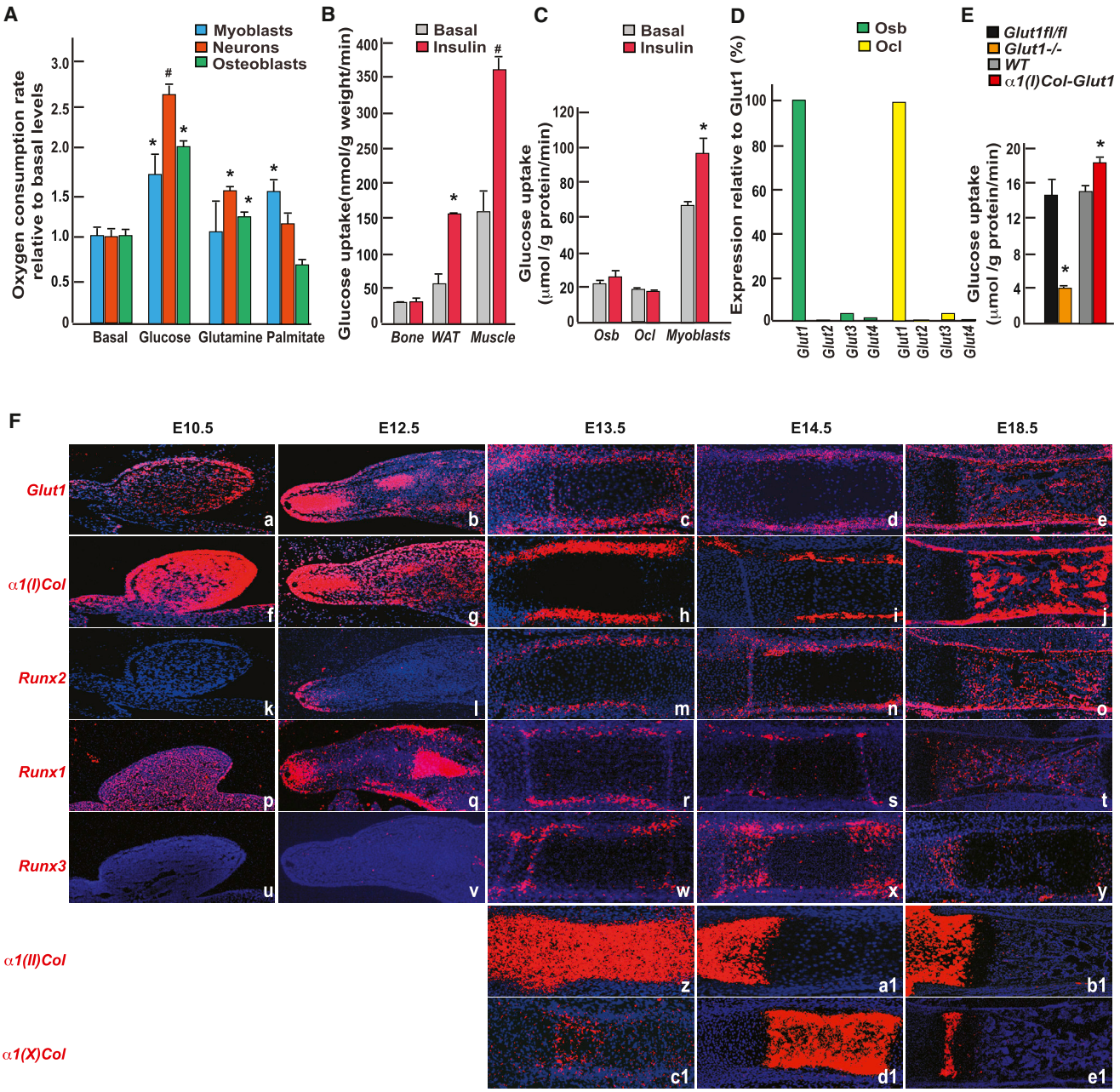

Figure 1. Insulin-Independent Glucose Uptake in Osteoblasts

(A) Oxygen consumption rate (OCR) of osteoblasts, C2C12 myoblasts, or hippocampal neurons incubated with vehicle, 10 mM glucose, 2 mM glutamine, or 300 μM palmitate in 1× Krebs-Henseleit buffer for 2 hr (n = 8).

(B) Glucose uptake measured by euglycemic hyperinsulinemic clamps in femurs, white adipose tissue, and gastrocnemius muscle of WT mice before or after insulin infusion (2.5 mU/kg/min) (n = 4).

(C) Uptake rate of 2-DG in osteoblasts (Osb), osteoclasts (Ocl), and myoblasts (n = 3).

(D) Expression of class I *Gluts* in osteoblasts and osteoclasts assayed by qPCR.

(E) Uptake rate of 2-DG in *Glut1fl/fl*, *Glut1−/−*, WT, and *α1(I)Col-Glut1* osteoblasts (n = 6–8).

(F) In situ hybridization analysis of *Glut1* (a–e), *α1(I) Collagen* (f–j), *Runx2* (k–o) *Runx1* (p–t), *Runx3* (u–v), *α1(II) Collagen* (z–b1), and *α1(X) Collagen* (c1–e1) in hindlimbs during embryonic development.

All error bars represent SEM.

See also Figure S1.

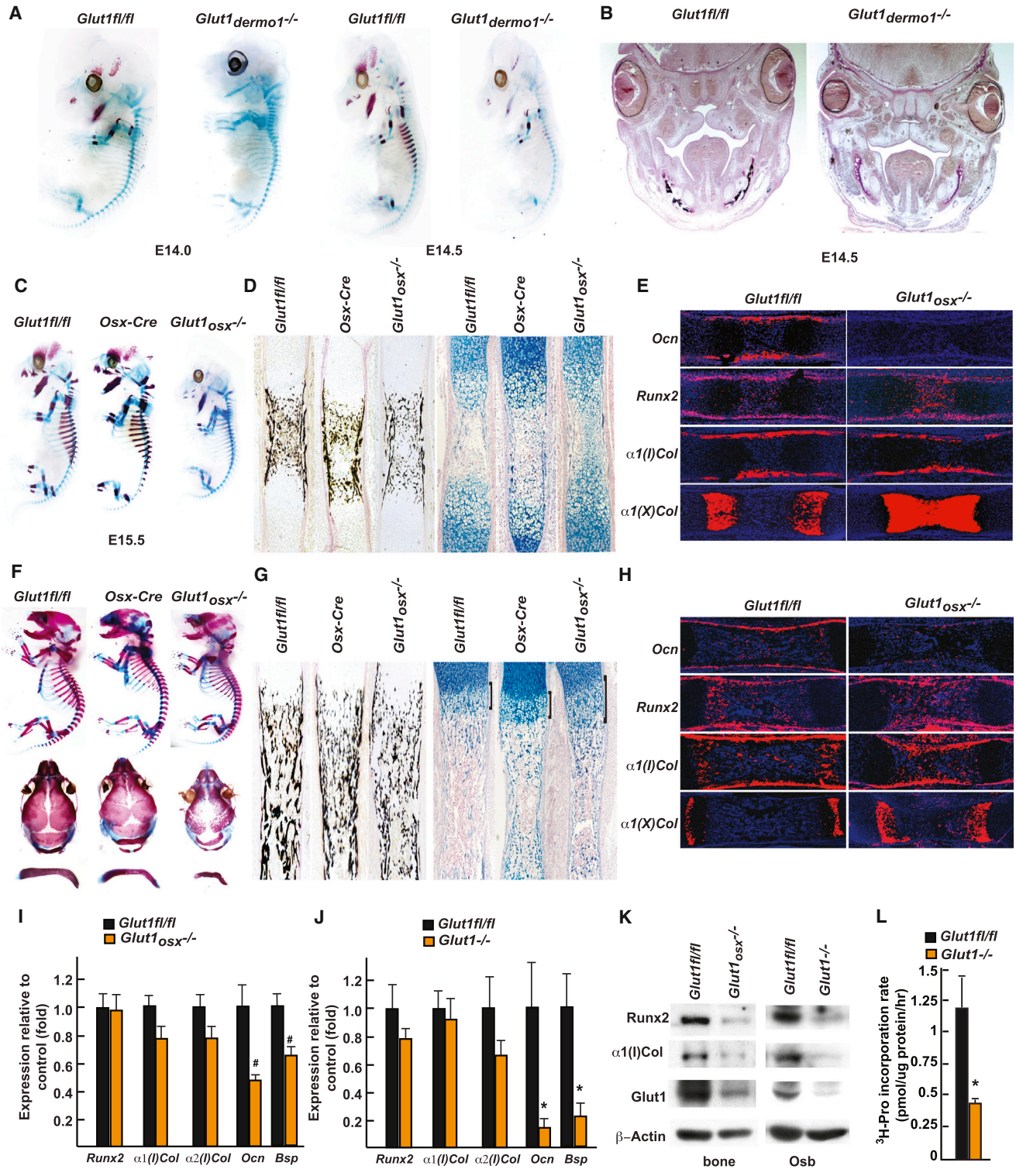

Figure 2. Glucose Uptake Is Necessary for Osteoblast Differentiation during Development

(A) Alcian blue/alizarin red staining of skeletal preparations of E14.0 and 14.5 *Glut1*$_{dermo1}$−/− and *Glut1fl/fl* embryos.

(B) Von Kossa staining of skull sections of E14.5 *Glut1*$_{dermo1}$−/− and *Glut1fl/fl* embryos.

(C) Alcian blue/alizarin red staining of skeletal preparations of E15.5 *Glut1*$_{osx}$−/−, *Glut1fl/fl*, and *Osx-cre* embryos.

(D) Von Kossa or alcian blue staining of femur from E15.5 *Glut1*$_{osx}$−/−, *Glut1fl/fl*, and *Osx-cre* embryos.

(E) In situ hybridization analysis of *Osteocalcin*, *α1(I)*, *α1(X) Collagen*, and *Runx2* expression in E15.5 *Glut1*$_{osx}$−/− and *Glut1fl/fl* femurs.

(legend continued on next page)

features are characteristic of CCD, a disease caused by the decreased function of RUNX2 (Mundlos et al., 1997; Lee et al., 1997), *Runx2* expression was normal in E18.5 *Glut1*$_{osx}$−/− bones. The same was true for *α1(I) Collagen* expression (Figures 2H–2J).

Accounting for this delay in osteoblast differentiation and CCD phenotype, there was a 70% decrease in RUNX2 accumulation in E18.5 *Glut1*$_{osx}$−/− bones and osteoblasts (Figure 2K). This decrease in RUNX2 accumulation was not observed for other transcription factors (Figure S2G). There was also a 70% decrease in type I collagen accumulation in E18.5 *Glut1*−/− bones and osteoblasts because of a 60% decrease in the rate of collagen synthesis in *Glut1*−/− compared to control osteoblasts (Figures 2K and 2L). This latter finding explained the decreased bone formation in *Glut1*$_{osx}$−/− embryos. Of note, *Chrebp*, a transcriptional mediator of glucose signaling in other cell types (Yamashita et al., 2001), is not expressed and does not regulate glucose uptake in osteoblasts (Figures S2H–S2K).

Glucose Uptake in Osteoblasts Is Necessary for Bone Formation and Whole-Body Glucose Homeostasis Post-natally

To study *Glut1* functions in osteoblasts post-natally, we crossed *Glut1fl/fl* mice with *Osteocalcin-Cre* mice (*Glut1*$_{ocn}$−/−) that do not initiate gene deletion before E18.5 (Zhang et al., 2002) and performed an inducible deletion of *Glut1* in osteoblasts in 6-week-old *Osx-Cre;Glut1fl/fl* mice (*Glut1*$_{Dox}$−/−). After verifying the specificity and efficiency of the gene deletions (Figures S3A and S3B), we examined both models of *Glut1*−/− mice at 3 months of age and included in this analysis *α1(I)Col-Glut1* mice that modestly overexpress (1.75-fold) *Glut1* in osteoblasts (Figure S2D).

Glut1$_{ocn}$−/− and *Glut1*$_{Dox}$−/− mice of either sex presented with a low bone mass in all bones analyzed, whereas *α1(I)Col-Glut1* mice displayed a high bone mass. In these mouse models, only the parameters of bone formation, i.e., circulating levels of PINP, mineral apposition rate, bone formation rate, and number of osteoblasts, were affected (Figures 3A–3C and S3C–S3E). Expression of the cell-cycle regulators *Ccnd2*, *Ccne1*, and *Cdk4* and osteoblast proliferation as measured by bromodeoxyuridine (BrdU) incorporation were decreased in *Glut1*$_{ocn}$−/− and increased in *α1(I)Col-Glut1* bones (Figures 3D and 3E). Again, accumulation, and not expression, of RUNX2 and type I collagen was decreased in *Glut1*$_{ocn}$−/− and increased in *α1(I)Col-Glut1* bones (Figures 3F and 3G).

Following fluctuating RUNX2 accumulation, expression of *Osteocalcin*, a RUNX2 target gene, and circulating osteocalcin levels were low in *Glut1*$_{ocn}$−/− mice and high in *α1(I)Col-Glut1* compared to control mice (Figures 3F and S3F). As a result, insulin secretion after glucose stimulation, glucose tolerance measured by a glucose tolerance test, insulin sensitivity assessed by an insulin tolerance test (ITT), and the steady-state glucose infusion rate during euglycemic-hyperpinsulinemic clamp were suppressed in *Glut1*$_{ocn}$−/− mice and improved in *α1(I)Col-Glut1* compared to control mice (Figures 3H–3N). In summary, glucose uptake in the cells of the osteoblast lineage is necessary for osteoblast differentiation, bone formation, and whole-body glucose homeostasis.

Glucose Uptake Favors Osteoblast Differentiation and Bone Formation by Inhibiting AMPK

To determine if the delay in osteoblast differentiation and the decrease in bone formation seen in *Glut1*$_{osx}$−/− embryos and mice were due to a decrease in protein synthesis that a poor glucose uptake triggers (Jeyapalan et al., 2007; Mayer et al., 2011), we measured AMP, ADP, and ATP contents in *Glut1*−/− osteoblasts.

Although AMP and ATP levels were not affected, there was a 3-fold increase in ADP content, leading to a 3-fold increase in the ratio of ADP to ATP in *Glut1*−/− versus control osteoblasts (Figures 4A and S4A). As a result, AMPK activity, assessed by the phosphorylation of its α subunit at Thr172 and of its substrate ACC1 at Ser79 (Woods et al., 1994; Wilson et al., 1996), was increased (Figure 4B). Several lines of evidence indicated that the activity of the mTORC1 complex was decreased in *Glut1*−/− osteoblasts. Phosphorylation of the mTORC1 substrates p70S6K at Thr389, 4E-BP1 at Thr37, and eIF4G at Ser1108 was decreased (Bolster et al., 2002; Reiter et al., 2005) (Figure 4C); Raptor phosphorylation at Ser792 was increased; and mTORC1 kinase activity was decreased in *Glut1*−/− osteoblasts (Figures 4B and 4D). Conversely, p70S6K phosphorylation and collagen accumulation were both decreased in *Raptor*−/− osteoblasts, and knockdown of *Tsc1* and *Tsc2* not only restored mTORC1 activity as measured by p70S6K phosphorylation but also normalized collagen accumulation in *Glut1*−/− osteoblasts (Figures 4E and 4F).

To demonstrate that the decrease in mTORC1 activity and the phenotypes of the *Glut1*$_{osx}$−/− mice are caused by an increase in AMPK activity in osteoblasts, we decreased the expression of *Ampk* in osteoblasts by generating *Glut1*−/− embryos or mice lacking in osteoblasts one allele of *Ampkα1*, the most highly expressed AMPKα subunit in these cells (Figure 4G). Phosphorylation of AMPKα1 and p70S6K, ATP contents, RUNX2, and type I collagen accumulations were similar in *Glut1*$_{osx}$−/−;*Ampka1*$_{osx}$+/− and control osteoblasts, indicating that AMPK activity and therefore mTORC1 signaling had been restored in *Glut1*$_{osx}$−/−;*Ampka1*$_{osx}$+/− osteoblasts (Figures 4H, S4B, and

(F) Alcian blue/alizarin red staining of skeletal preparations of E18.5 *Glut1*$_{osx}$−/−, *Glut1fl/fl*, and *Osx-cre* embryos.
(G) Von Kossa or alcian blue staining of femur from E18.5 *Glut1*$_{osx}$−/−, *Glut1fl/fl*, and *Osx-cre* embryos.
(H) In situ hybridization analysis of *Osteocalcin*, *α1(I)*, *α1(X) Collagen*, and *Runx2* expression in E18.5 *Glut1*$_{osx}$−/− and *Glut1fl/fl* femurs.
(I) Expression of osteoblast markers in E18.5 *Glut1*$_{osx}$−/− and *Glut1fl/fl* femurs (n = 9).
(J) Expression of osteoblast marker genes in *Glut1fl/fl* and *Glut1*−/− osteoblasts (n = 6).
(K) α1(I) Collagen and RUNX2 accumulations in E18.5 *Glut1*$_{osx}$−/− and *Glut1fl/fl* femurs and *Glut1fl/fl* and *Glut1*−/− osteoblasts.
(L) ^{3}H-proline incorporation into collagen of *Glut1fl/fl* and *Glut1*−/− osteoblasts (n = 6).
All error bars represent SEM.
See also Figure S2.

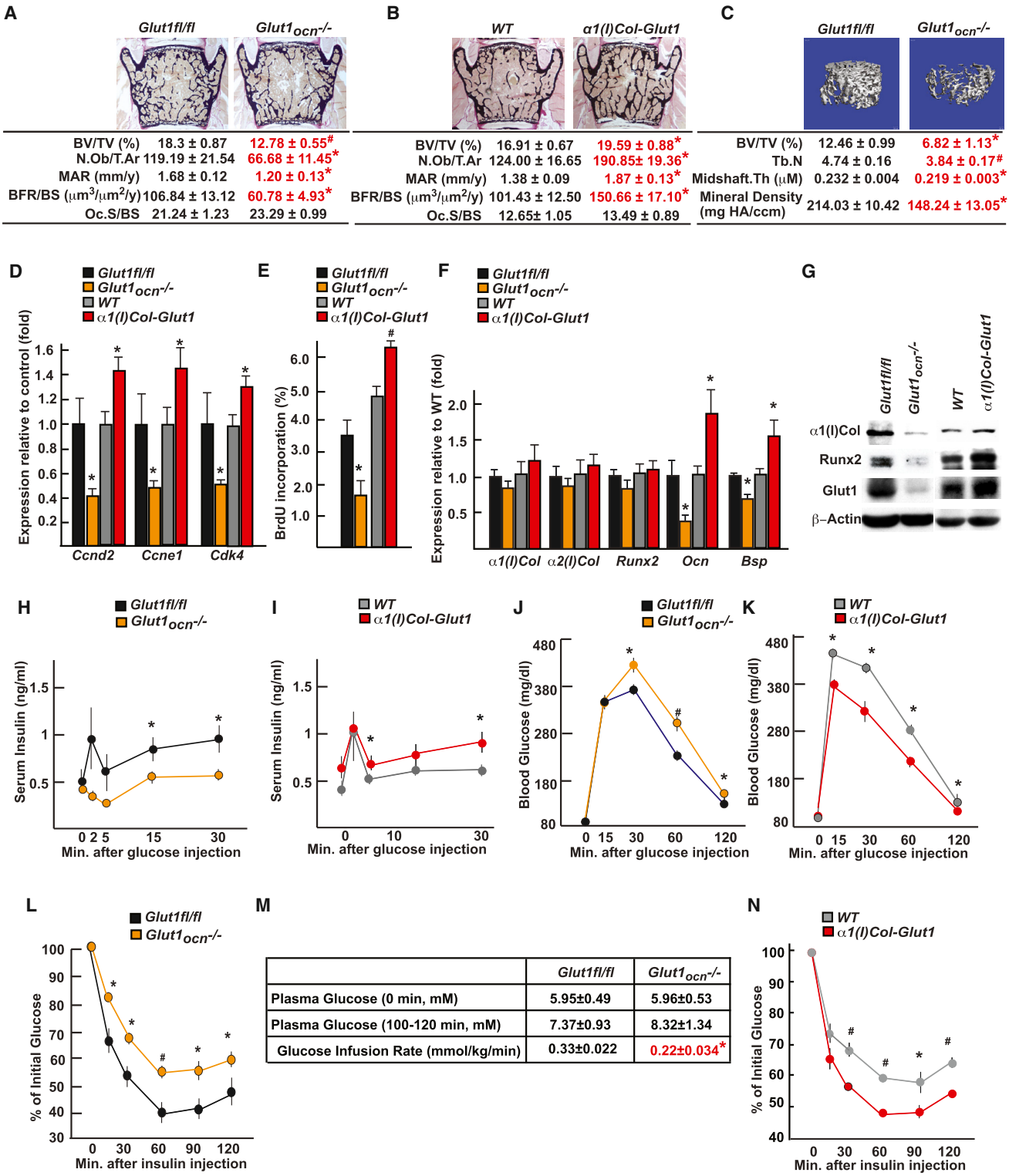

Figure 3. Glucose Uptake in Osteoblasts Is Necessary for Bone Formation and Glucose Homeostasis Post-natally

(A and B) Histomorphometric analysis of L4 vertebrae of 3-month-old *Glut1fl/fl*, *Glut1*$_{ocn}$−/−, WT, and *α1(I)Col-Glut1* male mice (n = 9–11).

(C) μCT analysis of proximal femurs of *Glut1fl/fl* and *Glut1*$_{ocn}$−/− male mice (n = 7).

(D) Expression of *Ccnd2*, *Ccne1*, and *Cdk4* in femurs of 3-month-old *Glut1fl/fl*, *Glut1*$_{ocn}$−/−, WT, and *α1(I)Col-Glut1* mice (n = 6).

(E) BrdU incorporation in calvaria of P14 *Glut1fl/fl*, *Glut1*$_{ocn}$−/−, WT, and *α1(I)Col-Glut1* mice (n = 5–8).

(legend continued on next page)

S4C). As a result, alcian blue/alizarin red staining of skeletal preparations, histological, and in situ hybridization analyses showed normal osteoblast differentiation and no evidence of CCD in *Glut1*$_{osx}$−/−;*Ampka1*$_{osx}$+/− embryos (Figures 4I–4L). Bone formation parameters were also normal in *Glut1*$_{ocn}$−/−;*Ampka1*$_{ocn}$+/− mice (Figure 4M).

Two experiments showed that increasing AMPK activity in osteoblasts is deleterious for bone. Treating mouse osteoblasts with AICAR, an AMPK agonist, profoundly decreased type I collagen and RUNX2 accumulations in these cells, and WT mice treated with AICAR from 6 to 14 weeks of age showed a significant decrease in bone formation parameters and bone mass (Figures 4N and 4O). Accordingly, and as is the case for *Glut1*−/− osteoblasts, WT osteoblasts deprived of glucose had higher levels of P-AMPK and lower levels of P-P70S6K and type I collagen than if cultured in the presence of glucose (Figure S4D).

Runx2 Cannot Induce Osteoblast Differentiation when Glucose Uptake Is Hampered

In the course of these experiments, we noticed that RUNX2 accumulation was restored when *Glut1*−/− osteoblasts were treated with an inhibitor of proteasome degradation and that RUNX2 ubiquitination was increased in *Glut1*−/− osteoblasts (Figure 5A). Normal RUNX2 ubiquitination in *Glut1*−/−;*Ampka1*+/− and *Glut1*−/−;*Ampka1*−/− osteoblasts (Figure 5B) implicated AMPK in RUNX2 polyubiquitination. Mass spectrometry and bioinformatics analyses identified a possible AMPK recognition site in SMURF1, an E3 ubiquitin ligase involved in RUNX2 degradation (Zhao et al., 2003) (Figures S5A and S5B). In vitro, AMPK phosphorylated SMURF1 at Ser148, and this phosphorylation event was needed for SMURF1-induced RUNX2 ubiquitination (Figures 5C and 5D). SMURF1 phosphorylation at Ser148 did not increase in *Ampka1*−/− osteoblasts, and RUNX2 accumulation did not decrease in *Ampka1*−/− or *Smurf1*−/− osteoblasts cultured in the absence of glucose as it did in WT osteoblasts (Figures 5E and 5F). Moreover, an anti-phospho-SMURF1 antibody demonstrated AMPKα1 interaction with phospho-SMURF1 in *Glut1*−/− osteoblasts and that SMURF1 phosphorylation at S148 was higher in *Glut1*−/− than in control, *Glut1*−/−;*Ampka1*+/−, and *Glut1*−/−;*Ampka1*−/− osteoblasts (Figures 5G and 5H). These results indicate that AMPK favors RUNX2 proteasomal degradation by phosphorylating SMURF1.

This unanticipated regulation of RUNX2 ubiquitination by AMPK allowed selectively assessing the ability of RUNX2 to induce osteoblast differentiation when glucose uptake is compromised. This was achieved by generating *Glut1*$_{osx}$−/− embryos and *Glut1*$_{ocn}$−/− mice lacking one allele of *Smurf1*. This manipulation normalized RUNX2 accumulation but did not restore mTORC1 signaling since p70S6K phosphorylation and type I collagen synthesis remained low in *Glut1*$_{osx}$−/−;*Smurf1*+/− osteoblasts (Figures 5I and 5J). As a result, and despite a normal accumulation of RUNX2, skeletal development was equally delayed in *Glut1*$_{osx}$−/−;*Smurf1*+/− and *Glut1*$_{osx}$−/− embryos at E15.5 and E18.5 (Figures 5K and 5L). The cartilaginous area and the zone of *α1(X)Col*-expressing cells were as enlarged in *Glut1*$_{osx}$−/−;*Smurf1*+/− embryos as in *Glut1*$_{osx}$−/− embryos (Figures 5M and 5N). Hence, RUNX2 cannot induce proper osteoblast differentiation during embryogenesis if glucose uptake is hampered because protein synthesis is decreased (Figure 5O). Likewise, *Glut1*$_{ocn}$−/−;*Smurf1*+/− mice were as osteopenic as *Glut1*$_{ocn}$−/− mice (Figure S5C).

Glucose Can Initiate Bone Formation in *Runx2*-Deficient Embryos

Next, we asked if conversely, raising the extracellular concentration of glucose was sufficient to initiate type I collagen synthesis in *Runx2*-deficient osteoblasts. To that end, *Runx2fl/fl* osteoblasts (Takarada et al., 2013) were infected with a *Cre*-expressing adenovirus (Figure S6A); these *Runx2*-/- osteoblasts were then cultured in a differentiation medium containing either 5 or 10 mM glucose.

In *Runx2*−/− osteoblasts cultured in the presence of 5 mM glucose, GLUT1 accumulation and glucose consumption rate were decreased, phosphorylation of AMPKα1 was high, and phosphorylation of p70S6K was low, indicating that mTORC1 signaling was inhibited. As a result, ^{3}H-proline incorporation into collagen molecules and accumulation of type I collagen were both lower in *Runx2*−/− than in control osteoblasts (Figures 6A–6C). In contrast, when the glucose concentration in the culture medium of *Runx2*−/− cells reached 10 mM, the glucose consumption rate doubled, and phosphorylation of AMPKα1 and p70S6K, the incorporation rate of ^{3}H-proline into collagen molecules, and the accumulation of type I collagen were normalized in *Runx2*−/− cells, even though *type I Collagen* gene expression did not changed (Figures 6A–6D).

In view of these results, we asked whether chronic hyperglycemia would improve bone formation in *Runx2*+/− embryos. This was achieved by injecting streptozotocin (STZ; 150 mg/kg) into *Runx2*+/− female mice as soon as a vaginal plug was seen. By decreasing the number of β cells and circulating insulin levels, this manipulation caused a severe hyperglycemia in E18.5 embryos (Figure 6E). We focused our analysis on bones forming through intramembranous ossification because they are the ones in which osteoblast differentiation is hampered by *Runx2*

(F) Expression of osteoblast marker genes in the femurs of 3-month-old *Glut1fl/fl*, *Glut1*$_{ocn}$−/−, WT, and *α1(I)Col-Glut1* mice (n = 8).
(G) α1(I) Collagen and RUNX2 accumulations in the femurs of 3-month-old *Glut1fl/fl*, *Glut1*$_{ocn}$−/−, WT, and *α1(I)Col-Glut1* mice.
(H and I) Glucose-stimulated insulin secretion in 3-month-old *Glut1fl/fl*, *Glut1*$_{ocn}$−/−, WT, and *α1(I)Col-Glut1* mice (n = 10–11).
(J and K) Glucose tolerance test in 3-month-old *Glut1fl/fl*, *Glut1*$_{ocn}$−/−, WT, and *α1(I)Col-Glut1* mice (n = 5–10).
(L) ITT in 3-month-old *Glut1fl/fl*, *Glut1*$_{ocn}$−/−, and WT mice (n = 8–10).
(M) Glucose infusion rate in 3-month-old *Glut1fl/fl* and *Glut1*$_{ocn}$−/− mice (n = 6).
(N) ITT in 3-month-old WT and *α1(I)Col-Glut1* mice (n = 8–10).
All error bars represent SEM.
See also Figure S3.

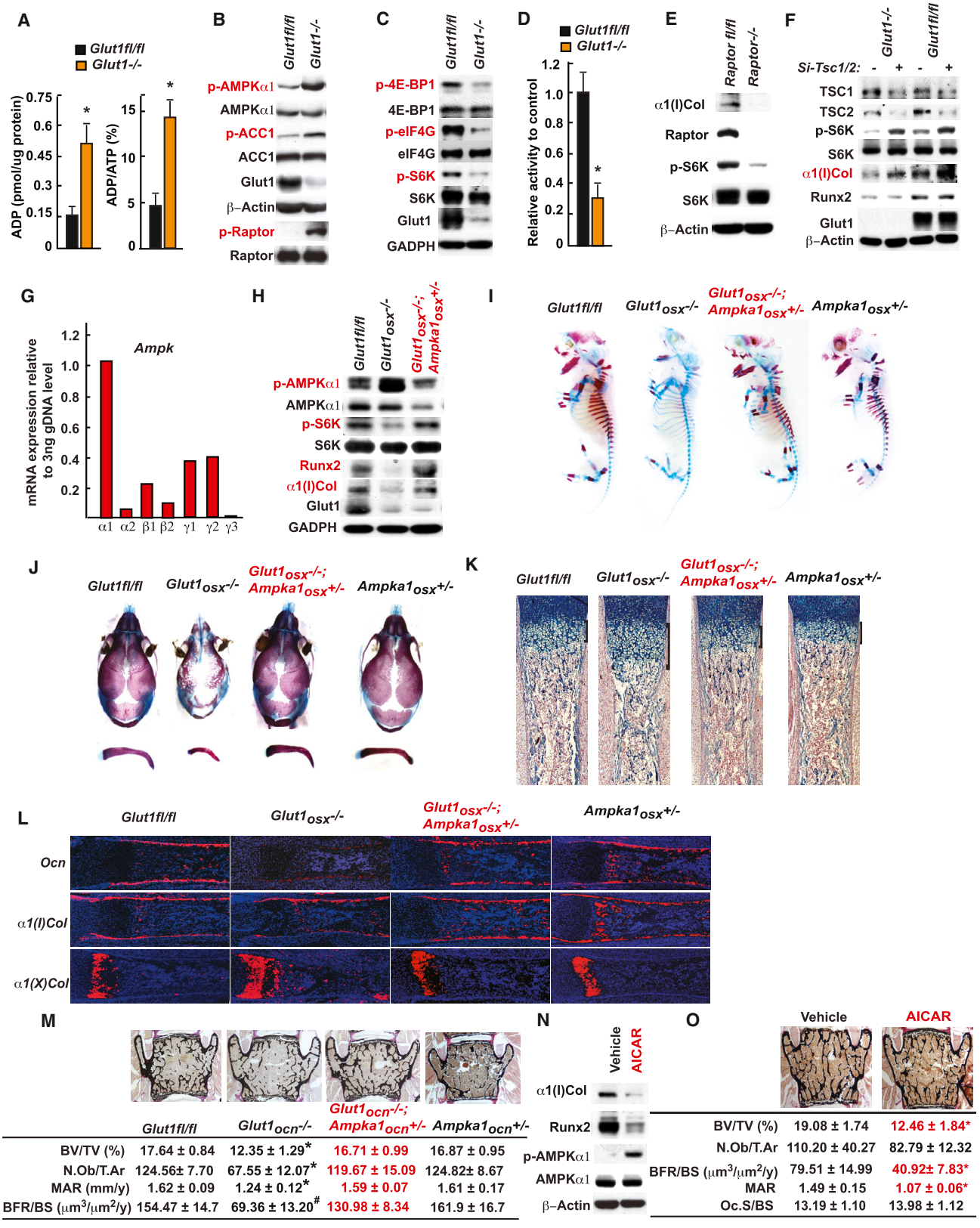

	Glut1fl/fl	Glut1ocn-/-	Glut1ocn-/-; Ampka1ocn+/-	Ampka1ocn+/-
BV/TV (%)	17.64 ± 0.84	12.35 ± 1.29*	16.71 ± 0.99	16.87 ± 0.95
N.Ob/T.Ar	124.56± 7.70	67.55 ± 12.07*	119.67 ± 15.09	124.82± 8.67
MAR (mm/y)	1.62 ± 0.09	1.24 ± 0.12*	1.59 ± 0.07	1.61 ± 0.17
BFR/BS ($\mu m^3/\mu m^2/y$)	154.47 ± 14.7	69.36 ± 13.20#	130.98 ± 8.34	161.9 ± 16.7

	Vehicle	AICAR
BV/TV (%)	19.08 ± 1.74	12.46 ± 1.84*
N.Ob/T.Ar	110.20 ± 40.27	82.79 ± 12.32
BFR/BS ($\mu m^3/\mu m^2/y$)	79.51 ± 14.99	40.92± 7.83*
MAR	1.49 ± 0.15	1.07 ± 0.06*
Oc.S/BS	13.19 ± 1.10	13.98 ± 1.12

(legend on next page)

haplo-insufficiency. While no difference was seen in WT embryos carried by STZ-treated mothers (Figure S6B), alcian blue/alizarin red staining of skeletal preparations showed that clavicles of E18.5 *Runx2*+/− embryos carried by STZ-treated mothers were twice as long as those of *Runx2*+/− embryos carried by vehicle-treated mothers (1.78 ± 0.08 mm and 0.85 ± 0.05 mm). Interparietal bones were also 2-fold larger in *Runx2*+/− embryos carried by STZ-treated mothers (2.09 ± 0.12 mm^2 and 1.01 ± 0.13 mm^2) than in those carried by control mothers, and the fontanelles of these embryos were less open than were those of *Runx2*+/− embryos carried by vehicle-treated mothers (Figures 6F and 6G). Histological analyses showed the presence of mineralized bone trabeculae in the clavicles of E18.5 *Runx2*+/− embryos carried by STZ-treated mothers (Figures 6H and 6I). An immunohistochemistry analysis showed the presence of type I collagen molecules in the clavicles of *Runx2*+/− embryos carried by STZ-treated mothers, whereas only type X collagen molecules were present in those of *Runx2*+/− embryos carried by vehicle-treated mothers (Figure 6J). Accumulation of type I collagen was also increased in the long bones of *Runx2*+/− embryos carried by STZ-treated mothers (Figures 6K and 6L). To further link the rescue of bone phenotype in *Runx2*-deficient embryos to the increase in blood glucose levels, we repeated this experiment using lower doses of STZ (50 or 100 mg/kg). One hundred milligram per kilogram of STZ was toxic for β cells since it decreased circulating insulin levels nearly 2-fold without raising blood glucose levels in the mothers or embryos (Figure 6E). This STZ dose did not correct the delay in bone development of *Runx2*-deficient embryos (Figures 6F and 6G). Thus, raising blood glucose levels normalized collagen synthesis and enhanced bone formation in *Runx2*+/− osteoblasts and embryos.

Although type I collagen accumulation was also normalized in skeletal elements obtained from *Runx2*−/− embryos carried by STZ-treated mothers (Figure 6M), alcian blue/alizarin red staining of skeletal preparations failed to show any ECM mineralization in the skeletons of E18.5 *Runx2*−/− embryos carried by STZ-treated mothers (Figure S6C). This is probably explained by the fact that RUNX2 regulates the expression of *Alkaline Phosphatase* (*Akp2*), a gene necessary for bone mineralization (Murshed et al., 2005) (Figures 6D and 6N).

Crosstalk between *Runx2* and *Glut1* Coordinates Osteoblast Differentiation and Bone Formation

The results presented above delineated the influence of glucose uptake on osteoblast differentiation and bone formation but did not explain how these two events are coordinated in vivo. In addressing this question we interpreted the fact that *Glut1* expression and glucose uptake were decreased in *Runx2*+/− bones (Figures 7A and 7B) as suggesting that RUNX2 regulates *Glut1* expression. *Runx1* expression in *Glut1*/*α1(I) Collagen*-expressing cells of the limb buds prompted us to test if Runx1 could trans-activate the *Glut1* promoter.

The *Glut1* promoter of the mouse and other vertebrate species has a canonical Runx binding site at −811 bp (Figure 7C). Chromatin immunoprecipitation assays verified that RUNX2 binds to this site (Figure 7D), and DNA co-transfection experiments performed in COS cells showed that *Runx2* or *Runx1* expression vectors could increase the activity of a *Glut1* promoter-luciferase reporter construct (p*Glut1-Luc*) only if this site was intact (Figure 7E). In agreement with these results, expression of *Glut1* was decreased in *Runx2*−/− and increased in *Schnurri-3*−/− osteoblasts (*Shn3*−/−) that display an increase in RUNX2 activity (Jones et al., 2006) (Figures 7F and S7A). These results explain why glucose uptake and mTORC1 activity were decreased in *Runx2*−/− and increased in *Shn3*−/− osteoblasts (Figures 6B and 7G).

If the feedforward regulation between GLUT1-dependent glucose uptake and RUNX2 provides an explanation for the coordination of osteoblast differentiation and bone formation, $Glut1_{osx}$+/−;*Runx2*+/− embryos should display a delay in osteoblast differentiation similar to that of *Runx2*−/− embryos. Alcian blue/alizarin red staining of skeletal preparations showed that $Glut1_{osx}$+/−;*Runx2*+/− embryos were indistinguishable from *Runx2*−/− embryos until E16.5 (Figures 7H and S7B). At E18.5, clavicles were barely detectable, and most of the bones forming the skull were absent or severely hypoplastic in $Glut1_{osx}$+/−;*Runx2*+/− embryos (Figure 7I). Alcian blue staining

Figure 4. Glucose Uptake Favors Osteoblast Differentiation and Bone Formation by Inhibiting AMPK

(A) ADP content and ADP-to-ATP ratio in WT and *Glut1*−/− osteoblasts (n = 6).

(B and C) AMPK, ACC1, Raptor (B), p70S6K, 4E-BP1, and eIF4G phosphorylation in WT and *Glut1*−/− osteoblasts.

(D) Kinase assay of immune-precipitated mTORC1 complex in WT and *Glut1*−/− osteoblasts (n = 3).

(E) Raptor, p70S6K phosphorylation, and α1(I)Collagen accumulations in WT and *Raptor*−/− osteoblasts.

(F) TSC1, TSC2, and p70S6K phosphorylation, α1(I)Collagen, and RUNX2 accumulations in WT and *Glut1*−/− osteoblasts transfected with siRNAs targeting *Tsc1* and *Tsc2* or scrambled siRNA.

(G) Expression of various AMPK subunits in osteoblasts.

(H) AMPK and p70S6K phosphorylation, RUNX2, and α1(I)Collagen accumulations in *Glut1fl/fl*, $Glut1_{osx}$−/−, and $Glut1_{osx}$−/−;$Ampka1_{osx}$+/− osteoblasts.

(I and J) Alcian blue/alizarin red staining of skeletal preparations of E15.5 (I) and 18.5 (J) *Glut1fl/fl*, $Glut1_{osx}$−/−, $Ampka1_{osx}$+/− and $Glut1_{osx}$−/−;$Ampka1_{osx}$+/− embryos.

(K) Alcian blue staining of histological sections of femurs of E18.5 *Glut1fl/fl*, $Glut1_{osx}$−/−, $Ampka1_{osx}$+/−, and $Glut1_{osx}$−/−;$Ampka1_{osx}$+/− embryos.

(L) In situ hybridization analysis of *Osteocalcin*, *α1(I)*, *α1(II)*, and *α1(X) Collagen* expression in femurs of E18.5 *Glut1fl/fl*, $Glut1_{osx}$−/−, $Ampka1_{osx}$+/−, and $Glut1_{osx}$−/−;$Ampka1_{osx}$+/− embryos.

(M) Histomorphometric analysis of L4 vertebrae of 3-month-old of *Glut1fl/fl*, $Glut1_{ocn}$−/−, $Ampka1_{ocn}$+/−, and $Glut1_{ocn}$−/−;$Ampka1_{ocn}$+/− male mice (n = 7–10).

(N) AMPK phosphorylation, RUNX2, and α1(I)Collagen accumulations in osteoblasts treated with vehicle or AICAR (0.1 mM) for 16 hr.

(O) Histomorphometric analysis of L4 vertebrae of 3-month-old of WT mice treated with vehicle or AICAR (250 mg/kg/day) for 8 weeks (n = 6).

All error bars represent SEM.

See also Figure S4.

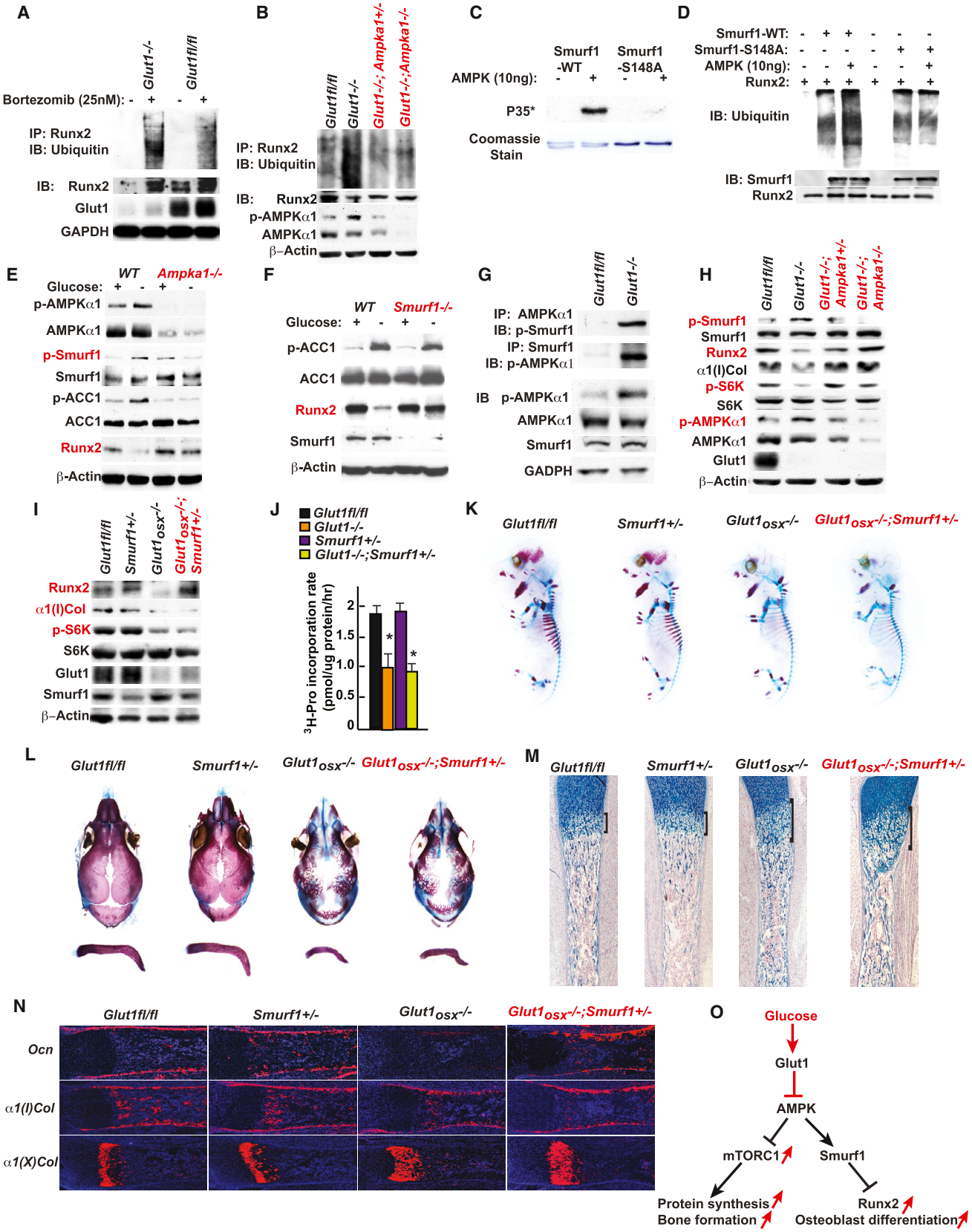

(legend on next page)

of histological sections of long bones showed an enlargement of the area of hypertrophic chondrocytes and a cartilaginous ECM in E18.5 *Glut1$_{osx}$+/−;Runx2+/−* embryos (Figure 7J). *Osteocalcin* expression was undetectable in E18.5 *Glut1$_{osx}$+/−;Runx2+/−* skeletal elements, while it was present in single heterozygous embryos. Conversely, the area covered by *α1(X) Collagen*-expressing cells was greatly enlarged in E18.5 *Glut1$_{osx}$+/−;Runx2+/−* embryos (Figure 7K). The extent of the delay in osteoblast differentiation in *Glut1$_{osx}$+/−;Runx2+/−* embryos and mice explained why they all died peri-natally. This crossregulation between *Runx2* and *Glut1* also determined the extent of bone formation since 3-month-old *Glut1$_{ocn}$+/−;Runx2+/−* mice had a low bone mass not seen in either *Glut1$_{ocn}$+/−* or *Runx2+/−* mice (Figure 7L).

Accounting for this severe phenotype, and in agreement with the feedforward loop between glucose uptake in osteoblasts and RUNX2, accumulation of GLUT1, type I collagen, and RUNX2 was decreased more than 80% and phosphorylation of AMPK and SMURF1 was increased in *Glut1$_{osx}$+/−;Runx2+/−* compared to single heterozygous bones (Figure 7M). Hence, crossregulation of RUNX2 and *Glut1* is an amplification mechanism that determines the onset of osteoblast differentiation and the extent of bone formation throughout life. We also treated *Runx2+/−* mothers with STZ (150 mg/kg) as soon as a vaginal plug was observed. This dose of STZ raised blood glucose levels in mothers and embryos (Figure S7C) and increased bone formation in skeletal elements of the skull and in clavicles in *Glut1$_{osx}$+/−;Runx2+/−* embryos (Figure 7N).

DISCUSSION

This study identifies glucose uptake in prospective osteoblasts as the earliest determinant of osteoblast differentiation and bone formation. It also shows that the coordination of osteoblast differentiation and bone formation throughout life is maintained by a feedforward regulation between glucose uptake in osteoblasts and RUNX2 accumulation. In addition, glucose uptake in osteoblasts is necessary for whole-body glucose homeostasis.

The Bases of the Coordination between Osteoblast Differentiation and Bone Formation

A striking feature of bone biology that has never been explained is that the synthesis of the main constituent of bone ECM, type I collagen, precedes the expression of, and is not regulated by, RUNX2, the earliest transcriptional determinant of osteoblast differentiation. This apparent disconnect between osteoblast differentiation and type I collagen synthesis in the bone could be explained by a single mechanism controlling both aspects of osteoblast biology and acting upstream of RUNX2. Our results suggest that this is the case and that this mechanism is glucose uptake in osteoblast progenitor cells. Glucose is the main nutrient of osteoblasts and is taken up by these cells in an insulin-independent manner through *Glut1*, whose expression precedes that of *Runx2*. Glucose uptake in osteoblasts favors osteoblast differentiation and bone formation through two distinct mechanisms. First, by inhibiting the activity of AMPK, glucose uptake enhances the activity of the mTORC1 pathway and therefore protein synthesis. Second, and unexpectedly, glucose uptake inhibits another function of AMPK documented here: its ability to favor RUNX2 ubiquitination in part via SMURF1. The two distinct functions of AMPK in osteoblasts revealed here explain why agonists of AMPK activity exert a deleterious influence on bone formation in vivo.

The *Glut1-Runx2* pathway described here could have clinical relevance. For instance, *Glut1$_{osx}$−/−* embryos develop CCD, a disease most often caused by a decrease in RUNX2 expression. However, a significant number of CCD patients do not have any detectable mutations in *Runx2* (Puppin et al., 2005; Tessa et al., 2003). Conceivably, in some of these patients, CCD may be caused by a decrease in glucose uptake or utilization in osteoblasts. If this were the case, it would further support the notion that skeletal dysplasia may have a nutritional basis (Elefteriou et al., 2006). Moreover, the predilection of osteoblasts for glucose demonstrated here provides a plausible explanation

Figure 5. Runx2 Cannot Induce Proper Osteoblast Differentiation if Glucose Uptake Is Hampered

(A) Ubiquitination of immune-precipitated RUNX2 in WT and *Glut1−/−* osteoblasts treated with 25 nM bortezomib for 16 hr.

(B) Ubiquitination of immune-precipitated RUNX2 in WT, *Glut1−/−*, *Glut1−/− Ampka1+/−*, and *Glut1−/− Ampka1−/−* osteoblasts treated with 25 nM bortezomib for 16 hr.

(C) In vitro AMPK phosphorylation assay of SMURF1 and SMURF1-S148/A.

(D) In vitro ubiquitination assay of Smurf1 and Smurf1-S148/A phosphorylated by AMPK.

(E and F) RUNX2 and α1(I)Collagen accumulations, AMPK, and SMURF1 phosphorylation in WT, *Smurf1−/−* (E), and *Ampka1−/−* (F) osteoblasts cultured with or without glucose for 16 hr.

(G) Co-immunoprecipitation of AMPKα1 and SMURF1 in WT and *Glut1−/−* osteoblasts.

(H) RUNX2 and α1(I)Collagen accumulations, AMPKα1, p70S6K, and SMURF1 phosphorylation in WT, *Glut1−/−*, *Glut1−/− Ampka1+/−*, and *Glut1−/− Ampka1−/−* osteoblasts.

(I) RUNX2 and α1(I)Collagen accumulations and p70S6K phosphorylation in *Glut1fl/fl*, *Glut1$_{osx}$−/−*, and *Glut1$_{osx}$−/−;Smurf1+/−* osteoblasts.

(J) ^{3}H-proline incorporation into collagen molecules of *Glut1fl/fl*, *Glut1−/−*, and *Glut1−/−;Smurf1+/−* osteoblasts (n = 6).

(K and L) Alcian blue/alizarin red staining of skeletal preparations of E15.5 (G) and 18.5 (I) *Glut1fl/fl*, *Smurf1+/−*, *Glut1$_{osx}$−/−*, and *Glut1$_{osx}$−/−;Smurf1+/−* embryos.

(M) Alcian blue staining of sections of femurs of E18.5 *Glut1fl/fl*, *Glut1$_{osx}$−/−*, and *Glut1$_{osx}$ −/−;Smurf1+/−* embryos.

(N) In situ hybridization analysis of *Osteocalcin*, *α1(I)*, and *α1(X) Collagens* expression in femurs of E18.5 *Glut1fl/fl*, *Glut1$_{osx}$−/−*, and *Glut1$_{osx}$−/−;Smurf1+/−* embryos.

(O) Schematic representation of the pathways triggered by glucose uptake in osteoblasts.

All error bars represent SEM.

See also Figure S5.

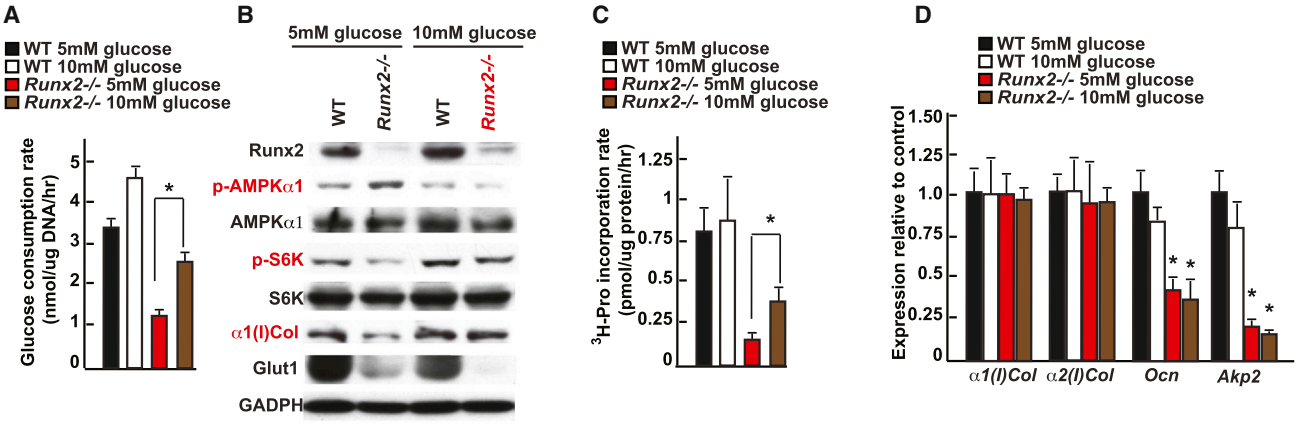

E

Blood Glucose (mg/dl)	Control	STZ (mg/kg)		
		50	100	150
Mothers	152.1 ± 11.7	155.3 ± 6.1	168.3 ±7.7	292.6 ± 17.2#
Runx2+/- fetus	50.5 ± 3.2	57.3 ±7.4	73.0 ±11.9	234.2 ± 26.4#
Runx2-/- fetus	48.3 ± 15.4	N.A	N.A	255.7 ± 29.3*
Serum Insulin (ng/ml)	Control	STZ50	STZ100	STZ150
Mothers	1.08 ± 0.08	0.98 ± 0.06	0.57 ± 0.05*	0.27 ± 0.05*

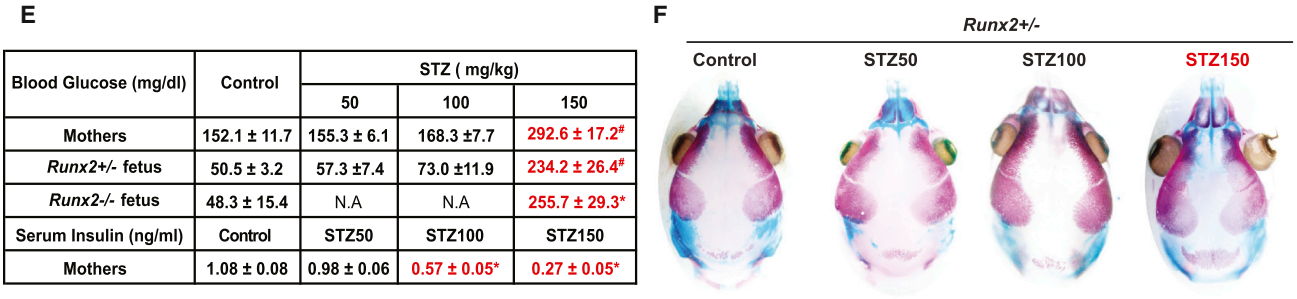

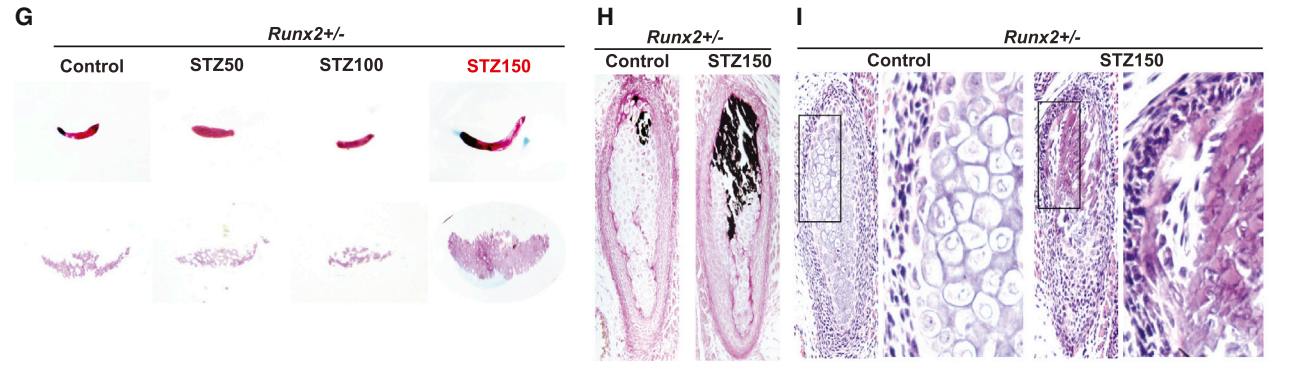

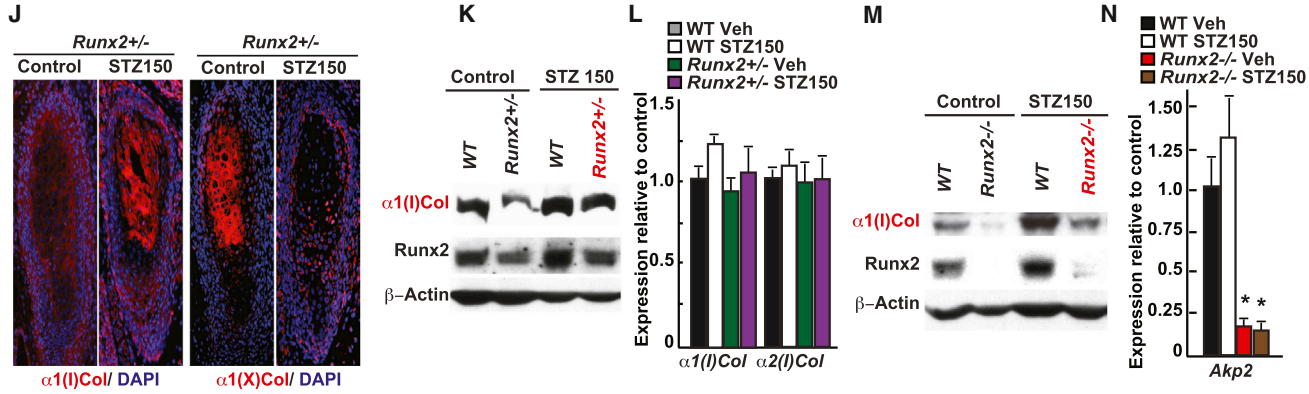

(legend on next page)

for why children chronically fed a ketogenic diet experience poor longitudinal growth (Groesbeck et al., 2006).

The Respective Functions of Glucose Uptake and Runx2 in Osteoblasts

Remarkably, restoring RUNX2 accumulation in *Glut1*−/− cells did not translate into efficient bone formation in vivo simply because in osteoblasts unable to properly take up glucose, protein synthesis remains low regardless of the level of expression of *Runx2*. On the other hand, raising the extracellular concentration of glucose was sufficient to initiate bone formation even though osteoblasts were not fully differentiated in *Runx2*+/− embryos. Raising blood glucose levels in *Runx2*−/− embryos also increased collagen synthesis but that did not translate into the presence of a mineralized bone ECM because expression of *Akp2*, a gene necessary for bone ECM mineralization, is low in the absence of *Runx2*. Thus, RUNX2 is necessary for osteoblast differentiation and bone ECM mineralization, but not for, paradoxically, the synthesis of the main constituent of this ECM. In broader terms, the importance of glucose uptake in osteoblast differentiation described here raises the hypothesis that glucose uptake may be a more general determinant of cell differentiation during embryonic development. This may be particularly relevant for tissue like muscle that uptakes large amounts of glucose.

Independently of its regulation of bone formation, glucose uptake in osteoblasts is necessary for another cardinal function of bone: the regulation of whole-body glucose metabolism. Indeed, through its regulation of RUNX2 accumulation, glucose favors expression of the hormone osteocalcin.

The Synergistic Functions of Glucose Uptake and Runx2 in Osteoblasts

How is osteoblast differentiation and bone formation coordinated throughout life? The fact that *Runx2*−/− and *Glut1*−/− osteoblasts had a similar metabolic profile suggested that this coordination might be explained if *Glut1* was a target gene of RUNX2.

In support of this hypothesis, both molecular and genetic evidence identifies RUNX2 as a major regulator of *Glut1* expression and glucose uptake in osteoblasts. As a result, *Runx2*−/− osteoblasts bear metabolic similarities with *Glut1*−/− osteoblasts; $Glut1_{osx}$+/−;*Runx2*+/− embryos are similar to *Runx2*−/− embryos; and $Glut1_{ocn}$+/−;*Runx2*+/− mice display an osteopenia not seen in either *Runx2*+/− or $Glut1_{ocn}$+/− mice. Hence, the reciprocal regulation between GLUT1-mediated glucose uptake and RUNX2 acts as an amplification chamber that determines the onset of osteoblast differentiation and the extent of bone formation throughout life. In addition, *Runx1* expression in the developing skeleton suggests that this Runx protein may regulate *Glut1* expression and thereby favor type I collagen accumulation in prospective osteoblasts before E12.5.

In broader terms, the results of this study cannot be separated from the recently described role of osteoblasts in maintaining glucose homeostasis in physiological and pathological situations (Lee et al., 2007; Ferron et al., 2010; Wei et al., 2014). The absolute necessity of glucose uptake for osteoblast differentiation, bone formation, and glucose homeostasis documented here illustrates, from the perspective of osteoblasts, the fundamental importance of crosstalk between bone and glucose metabolism.

EXPERIMENTAL PROCEDURES

Mice Generation

To generate *Glut1fl*/+ mice, a targeting vector harboring two LoxP sites flanking exons 3–10 of *Glut1* were electroporated into embryonic stem cells (ES cells) (CSL3,129/SvEvTac) (Figure S2A). Targeted ES cells were detected by Southern blots and injected in 129Sv/EV blastocysts to generate chimeric mice. Chimeric mice were crossed with Gt(ROSA)26Sor$^{tm1(FLP1)Dym}$ mice to remove the *Neomycin*-resistance cassette and to generate *Glut1fl*/+ mice. *Glut1fl*/+ mice were then crossed with *Dermo1-Cre* (Yu et al., 2003), *Osterix-Cre* (Rodda and McMahon, 2006), or *Ocn-Cre* mice (Zhang et al., 2002) to generate $Glut1_{osb}$+/− mice, whose progenies were intercrossed to obtain $Glut1_{dermo1}$−/−, $Glut1_{osx}$−/−, and $Glut1_{ocn}$−/− mice, respectively. To generate *α1(I)Col-Glut1* transgenic mice, a cDNA fragment of the mouse *Glut1* was cloned into a plasmid containing a 2.3-kb *α1(I)* collagen promoter and microinjected using standard protocols. *Ampka1fl/fl* mice were obtained from the Jackson Laboratory (Nakada et al., 2010). *Runx2fl/fl* mice were generated as previously described (Takarada et al., 2013). *Shn3*+/− and *Smurf1*+/− mice were generous gifts of Dr. L. Glimcher (Weill Cornell Medical College) and Dr. J. Wrana (University of Toronto, Canada), respectively (Jones et al., 2006; Narimatsu et al., 2009). Except for *α1(I)Col-Glut1* mice, which were backcrossed to a C57 background five times, all other mice analyzed were maintained on a C57/129 mixed background. Control littermates were analyzed in all experiments. All procedures involving animals were approved by CUMC IACUC and conform to the relevant regulatory standards.

Figure 6. Glucose Can Initiate Bone Formation in Runx2-Deficient Embryos

(A) Glucose consumption rate in WT and *Runx2*−/− osteoblasts cultured with 5 or 10 mM glucose for 16 hr.

(B) RUNX2, α1(I)Collagen, and GLUT1 accumulations, AMPKα1, and p70S6K phosphorylation in WT and *Runx2*−/− osteoblasts cultured with 5 or 10 mM glucose for 14 days.

(C) ^{3}H-proline incorporation into collagen molecules of WT and *Runx2*−/− osteoblasts cultured with 5 or 10 mM glucose for 14 days (n = 5).

(D) qPCR analysis of osteoblast marker genes in WT and *Runx2*−/− osteoblasts cultured with 5 or 10 mM glucose for 14 days (n = 6).

(E) Blood glucose and insulin levels in STZ (50, 100, and 150 mg/kg) and vehicle-treated *Runx2*+/− mothers and progenies at E18.5 (n = 5–12).

(F and G) Alcian blue/alizarin red staining of the skull (F), clavicles, and interparietal bones (G) of E18.5 *Runx2*+/− embryos carried by STZ (50, 100, or 150 mg/kg) and vehicle-treated mothers.

(H and I) Von Kossa/van Gieson staining (H) and H&E staining (I) of clavicles of E18.5 *Runx2*+/− embryos carried by STZ- (150 mg/kg) or vehicle-treated mothers.

(J) Immunohistochemical detection of type I and type X collagens in clavicles of E18.5 *Runx2*+/− embryos carried by STZ- (150 mg/kg) or vehicle-treated mothers.

(K) RUNX2 and α1(I)Collagen accumulations in femurs of E18.5 WT and *Runx2*+/− embryos carried by STZ- (150 mg/kg) or vehicle-treated mothers.

(L) *α1(I)* and *α2(I) Collagen* expression in femurs of E18.5 WT and *Runx2*+/− embryos carried by STZ- (150 mg/kg) or vehicle-treated mothers (n = 8).

(M) RUNX2 and α1(I)Collagen accumulations in femurs of E18.5 WT and *Runx2*−/− embryos carried by STZ- (150 mg/kg) or vehicle-treated mothers.

(N) *Akp2* expression in femurs of E18.5 of WT and *Runx2*−/− embryos carried by STZ- (150 mg/kg) or vehicle-treated mothers (n = 6).

All error bars represent SEM.

See also Figure S6.

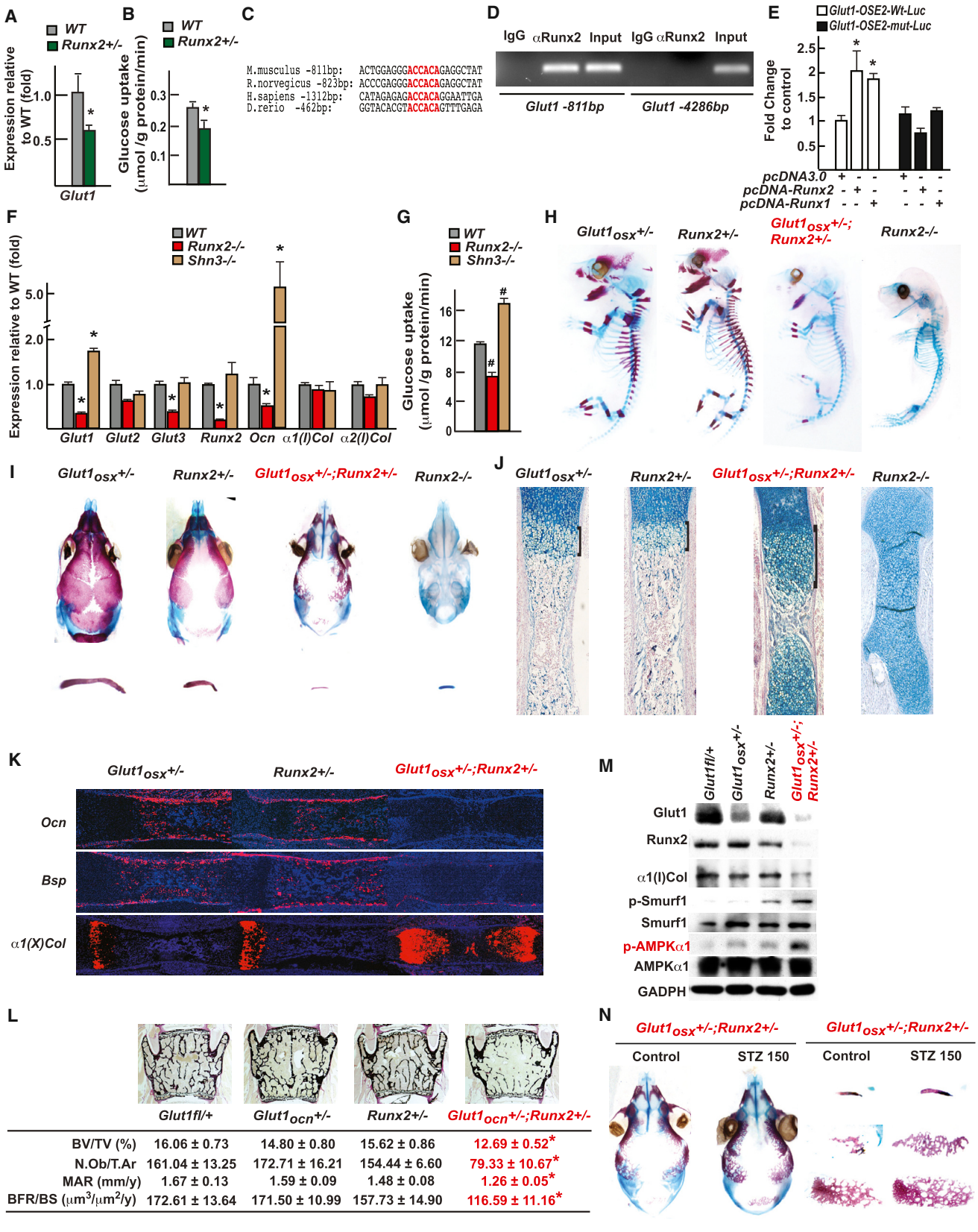

	Glut1fl/+	Glut1ocn+/-	Runx2+/-	Glut1ocn+/-;Runx2+/-
BV/TV (%)	16.06 ± 0.73	14.80 ± 0.80	15.62 ± 0.86	12.69 ± 0.52*
N.Ob/T.Ar	161.04 ± 13.25	172.71 ± 16.21	154.44 ± 6.60	79.33 ± 10.67*
MAR (mm/y)	1.67 ± 0.13	1.59 ± 0.09	1.48 ± 0.08	1.26 ± 0.05*
BFR/BS ($\mu m^3/\mu m^2/y$)	172.61 ± 13.64	171.50 ± 10.99	157.73 ± 14.90	116.59 ± 11.16*

(legend on next page)

Cell Culture

Mouse calvaria osteoblasts were isolated and cultured as described previously (Ducy and Karsenty, 1995). Osteoclast precursors (monocytes) were isolated by culturing bone marrow cells with αMEM/10% fetal bovine serum (FBS) containing M-CSF (10 ng/ml) for 6 days and then treated with RANKL (30 ng/ml) and M-CSF (10 ng/ml) for 7 days. C2C12 myoblasts (ATCC), the mHippoE-14 embryonic mouse hippocampal hypothalamic cell line (Cellutions Biosystems), and COS-7 cells were cultured in DMEM/10% FBS. *Glut1−/−*, *Raptor−/−*, *Runx2−/−*, *Glut1−/−;Ampka1+/−*, *Glut1−/−;Ampka1−/−*, *Ampka1+/−*, and *Ampka1−/−* calvaria osteoblasts were generated by infecting *Glut1fl/fl*, *Raptorfl/fl*, *Runx2fl/fl*, *Glut1fl/fl;Ampka1fl/+*, *Glut1fl/fl;Ampka1fl/fl*, *Ampka1fl/+*, or *Ampka1fl/fl* osteoblasts with either empty vector or *Cre*-expressing adenovirus (1:800 MOI) (University of Iowa). Small interfering RNAs (siRNAs) against *Tsc1* and *Tsc2* (Dharmacon) were transfected to primary osteoblasts, according to the manufacturer's protocol.

Molecular Biology and Biochemistry

For quantifying gene expression, RNA samples were extracted using TRIZOL reagent (Invitrogen). One to two micrograms of total RNA were converted into cDNA using M-MLV reverse transcriptase (Invitrogen). qPCR analyses were performed using CFX-Connect real-time PCR system (Bio-Rad). Relative expression levels of each gene were normalized to the levels of 18S rRNA or β-actin. Western blot analyses were carried out using standard protocols. All antibodies were obtained from Cell Signaling Technology, except for the anti-GLUT1 (EMD Millipore), anti-COL1A1, anti-RUNX2, anti-SMURF1 (Santa Cruz), anti-Phospho-Ser148 SMURF1 (Genescript), and anti-β-ACTIN (Sigma). Quantification of western blots was performed using ImageJ. Protein levels were quantified and normalized to ACTIN or GADPH levels. Relative protein levels were calculated with respect to control samples. All western blot experiments were repeated at least three times, with different samples.

Glucose Consumption and Uptake Assay

For glucose consumption measurements, following 16-hr incubation with osteoblasts, the glucose concentration in the culture medium was assayed with a Glucose Assay Kit (Biovision). Glucose uptake was determined by the uptake rate of 2-[U-^{14}C] deoxyglucose (2-DG) in cells. Following a 1-hr fast in glucose-free Krebs-Ringer HEPES (KRH) buffer (50 mM HEPES [pH 7.4], 136 mM NaCl, 4.7 mM KCl, 1.25 mM $MgSO_4$, 1.25 mM $CaCl_2$, and 0.1% BSA), cells were cultured in KRH buffer containing 100 μM 2-deoxyglucose and 0.5 μCi/ml 2-^{14}C-DG (287 mCi/mmol, Perkin Elmer, NEC495A) for 1 hr. For glucose uptake in bones, 10 μCi of 2-^{14}C-DG were immunoprecipitate injected in mice at a random feed state for 1 hr, and calvariae were then collected for analysis. The amount of 2-^{14}C-DG in total cell or bone lyses was quantified by liquid scintillation counter (WALLAC 1409) and normalized to protein content (Bio-Rad).

Skeleton Preparation, Bone Histology, and In Situ Hybridization

Skeleton preparations and alcian blue/alizarin red staining were carried out according to standard protocols (McLeod, 1980). Bone histology analyses, including Von Kossa staining and alcian blue staining, were performed with histological sections of femurs or clavicle bones using standard protocols. For all skeletal analyses, at least three litters for each embryonic stage and at least five embryos for each genotype were examined. Bone histomorphometry analyses were performed on L3 and L4 vertebrae as described previously (Chappard et al., 1987; Parfitt et al., 1987). Von Kossa/van Gieson staining, toluidine blue staining, and calcein double-labeling were performed to measure mineralized bone volume over the total tissue volume (BV/TV), osteoblast number per tissue area (N.Ob/T.Ar), mineralization apposition rate (MAR), and bone formation rate per bone surface (BFR/BS). For in situ hybridization, tissues were fixed in 4% paraformaldehyde/PBS overnight at 4°C and then embedded in paraffin after dehydration and sectioned at 5 μm. In situ hybridization was performed using ^{35}S-labeled riboprobe as described (Ducy et al., 1997). The *Runx1*, *Runx3*, *Runx2*, *α1(I)Col*, *α 1(II)Col*, *α 1(X)Col*, *Osteocalcin*, and *Bsp* probes have been previously described (Takeda et al., 2001). The *Glut1* probe is a 500-bp fragment of the *Glut1* 3′ UTR (see the Supplemental Experimental Procedures for sequence information). Hybridizations were performed overnight at 55°C, and washes were performed at 63°C.

Statistics

All data are presented as mean ± SEM. Statistical analyses were performed using unpaired, two-tailed Student's t test for comparison between two groups, and an ANOVA test was used for experiments involving more than two groups. For all experiments, * denotes $p \leq 0.05$, and # denotes $p \leq 0.001$ compared to control.

SUPPLEMENTAL INFORMATION

Supplemental Information includes Supplemental Experimental Procedures and seven figures and can be found with this article online at http://dx.doi.org/10.1016/j.cell.2015.05.029.

AUTHOR CONTRIBUTIONS

J.W. and G.K. conceived and designed the studies; J.W. and J.S. performed most experiments; M.P.M. generated the *Glut1fl/fl* mice; A.M. performed some histological analysis; D.K. performed the in vivo AICAR treatment experiment; H.Z. and J.E.P. performed glucose clamp analyses; T.T., T.L., and E.H. performed experiments using *Runx2−/−* osteoblasts; and J.W. and G.K. wrote the paper.

ACKNOWLEDGMENTS

We thank Drs. P. Ducy, J. Wrana, J. Shim, and L. Glimcher for their critical reading of the manuscript and reagents. This work was supported by the NIH (R01AR045548) (to G.K.), a Columbia University Mandl Connective Tissue Research Fellowship (to J.W.), and a Honjo International Scholarship (to J.S.).

Figure 7. The Reciprocal Regulation between Runx2 and Glut1 Determines Osteoblast Differentiation and Bone Formation

(A) *Glut1* expression in femurs of 3-month-old *Runx2+/−* mice (n = 8).
(B) Uptake rate of 2-DG in the calvaria of 6-week-old WT and *Runx2+/−* (n = 4–5) mice.
(C) Runx binding sites in the *Glut1* promoter of several species.
(D) Chromatin immunoprecipitation assay of RUNX2 binding to the promoter of mouse *Glut1*.
(E) Luciferase assay of *pGlut1*-WT-*Luc* or *pGlut1-mut-Luc* in COS cells co-transfected with RUNX2 or Runx1 expression vector (n = 6).
(F) Expression of osteoblast marker genes in WT, *Runx2−/−*, *and Shn3−/−* osteoblasts (n = 6).
(G) Glucose uptake in WT, *Runx2−/−*, *and Shn3−/−* osteoblasts measured by the uptake rate of 2-DG (n = 6).
(H and I) Alcian blue/alizarin red staining of skeletal preparations of E16.5 (H) and 18.5 (I) $Glut1_{osx}$*+/−*, *Runx2+/−*, $Glut1_{osx}$*+/−;Runx2+/−*, and *Runx2−/−* embryos.
(J) Alcian blue staining of histological sections of femurs of E18.5 $Glut1_{osx}$*+/−*, *Runx2+/−*, $Glut1_{osx}$*+/−;Runx2+/−*, and *Runx2−/−* embryos.
(K) In situ hybridization analysis of *Osteocalcin*, *Bsp*, and *α1(X) Collagen* expression in E18.5 $Glut1_{osx}$*+/−*, *Runx2+/−*, and $Glut1_{osx}$*+/−;Runx2+/−* femurs.
(L) Bone histomorphometric analysis of L4 vertebrae of 3-month-old of *Glut1fl/+*, $Glut1_{ocn}$*+/−*, *Runx2+/−*, and $Glut1_{ocn}$*+/−;Runx2+/−* female mice (n = 9–12).
(M) RUNX2 and α1(I)Collagen accumulations and AMPKα1 and SMURF1 phosphorylation in femurs of E18.5 *Glut1fl/+*, $Glut1_{osx}$*+/−*, *Runx2+/−*, and $Glut1_{osx}$*+/−;Runx2+/−* embryos.
(N) Alcian blue/alizarin red staining of skeletal preparations of E18.5 $Glut1_{osx}$*+/−;Runx2+/−* embryos carried by mothers treated with STZ (150 mg/kg) or vehicle.
All error bars represent SEM.
See also Figure S7.

Received: October 3, 2014
Revised: February 9, 2015
Accepted: April 9, 2015
Published: June 18, 2015

REFERENCES

Bolster, D.R., Crozier, S.J., Kimball, S.R., and Jefferson, L.S. (2002). AMP-activated protein kinase suppresses protein synthesis in rat skeletal muscle through down-regulated mammalian target of rapamycin (mTOR) signaling. J. Biol. Chem. *277*, 23977–23980.

Chappard, D., Palle, S., Alexandre, C., Vico, L., and Riffat, G. (1987). Bone embedding in pure methyl methacrylate at low temperature preserves enzyme activities. Acta Histochem. *81*, 183–190.

Ducy, P., and Karsenty, G. (1995). Two distinct osteoblast-specific cis-acting elements control expression of a mouse osteocalcin gene. Mol. Cell. Biol. *15*, 1858–1869.

Ducy, P., Zhang, R., Geoffroy, V., Ridall, A.L., and Karsenty, G. (1997). Osf2/Cbfa1: a transcriptional activator of osteoblast differentiation. Cell *89*, 747–754.

Elefteriou, F., Benson, M.D., Sowa, H., Starbuck, M., Liu, X., Ron, D., Parada, L.F., and Karsenty, G. (2006). ATF4 mediation of NF1 functions in osteoblast reveals a nutritional basis for congenital skeletal dysplasiae. Cell Metab. *4*, 441–451.

Ferrannini, E., Simonson, D.C., Katz, L.D., Reichard, G., Jr., Bevilacqua, S., Barrett, E.J., Olsson, M., and DeFronzo, R.A. (1988). The disposal of an oral glucose load in patients with non-insulin-dependent diabetes. Metabolism *37*, 79–85.

Ferron, M., Wei, J., Yoshizawa, T., Del Fattore, A., DePinho, R.A., Teti, A., Ducy, P., and Karsenty, G. (2010). Insulin signaling in osteoblasts integrates bone remodeling and energy metabolism. Cell *142*, 296–308.

Groesbeck, D.K., Bluml, R.M., and Kossoff, E.H. (2006). Long-term use of the ketogenic diet in the treatment of epilepsy. Dev. Med. Child Neurol. *48*, 978–981.

Jeyapalan, A.S., Orellana, R.A., Suryawan, A., O'Connor, P.M., Nguyen, H.V., Escobar, J., Frank, J.W., and Davis, T.A. (2007). Glucose stimulates protein synthesis in skeletal muscle of neonatal pigs through an AMPK- and mTOR-independent process. Am. J. Physiol. Endocrinol. Metab. *293*, E595–E603.

Jones, D.C., Wein, M.N., Oukka, M., Hofstaetter, J.G., Glimcher, M.J., and Glimcher, L.H. (2006). Regulation of adult bone mass by the zinc finger adapter protein Schnurri-3. Science *312*, 1223–1227.

Karsenty, G., Kronenberg, H.M., and Settembre, C. (2009). Genetic control of bone formation. Annu. Rev. Cell Dev. Biol. *25*, 629–648.

Kern, B., Shen, J., Starbuck, M., and Karsenty, G. (2001). Cbfa1 contributes to the osteoblast-specific expression of type I collagen genes. J. Biol. Chem. *276*, 7101–7107.

Lee, B., Thirunavukkarasu, K., Zhou, L., Pastore, L., Baldini, A., Hecht, J., Geoffroy, V., Ducy, P., and Karsenty, G. (1997). Missense mutations abolishing DNA binding of the osteoblast-specific transcription factor OSF2/CBFA1 in cleidocranial dysplasia. Nat. Genet. *16*, 307–310.

Lee, N.K., Sowa, H., Hinoi, E., Ferron, M., Ahn, J.D., Confavreux, C., Dacquin, R., Mee, P.J., McKee, M.D., Jung, D.Y., et al. (2007). Endocrine regulation of energy metabolism by the skeleton. Cell *130*, 456–469.

Long, F. (2012). Building strong bones: molecular regulation of the osteoblast lineage. Nat. Rev. Mol. Cell Biol. *13*, 27–38.

Mayer, F.V., Heath, R., Underwood, E., Sanders, M.J., Carmena, D., McCartney, R.R., Leiper, F.C., Xiao, B., Jing, C., Walker, P.A., et al. (2011). ADP regulates SNF1, the Saccharomyces cerevisiae homolog of AMP-activated protein kinase. Cell Metab. *14*, 707–714.

McLeod, M.J. (1980). Differential staining of cartilage and bone in whole mouse fetuses by alcian blue and alizarin red S. Teratology *22*, 299–301.

Mundlos, S., Otto, F., Mundlos, C., Mulliken, J.B., Aylsworth, A.S., Albright, S., Lindhout, D., Cole, W.G., Henn, W., Knoll, J.H., et al. (1997). Mutations involving the transcription factor CBFA1 cause cleidocranial dysplasia. Cell *89*, 773–779.

Murshed, M., Harmey, D., Millán, J.L., McKee, M.D., and Karsenty, G. (2005). Unique coexpression in osteoblasts of broadly expressed genes accounts for the spatial restriction of ECM mineralization to bone. Genes Dev. *19*, 1093–1104.

Nakada, D., Saunders, T.L., and Morrison, S.J. (2010). Lkb1 regulates cell cycle and energy metabolism in haematopoietic stem cells. Nature *468*, 653–658.

Narimatsu, M., Bose, R., Pye, M., Zhang, L., Miller, B., Ching, P., Sakuma, R., Luga, V., Roncari, L., Attisano, L., and Wrana, J.L. (2009). Regulation of planar cell polarity by Smurf ubiquitin ligases. Cell *137*, 295–307.

Parfitt, A.M., Drezner, M.K., Glorieux, F.H., Kanis, J.A., Malluche, H., Meunier, P.J., Ott, S.M., and Recker, R.R.; Report of the ASBMR Histomorphometry Nomenclature Committee (1987). Bone histomorphometry: standardization of nomenclature, symbols, and units. J. Bone Miner. Res. *2*, 595–610.

Puppin, C., Pellizzari, L., Fabbro, D., Fogolari, F., Tell, G., Tessa, A., Santorelli, F.M., and Damante, G. (2005). Functional analysis of a novel RUNX2 missense mutation found in a family with cleidocranial dysplasia. J. Hum. Genet. *50*, 679–683.

Reiter, A.K., Bolster, D.R., Crozier, S.J., Kimball, S.R., and Jefferson, L.S. (2005). Repression of protein synthesis and mTOR signaling in rat liver mediated by the AMPK activator aminoimidazole carboxamide ribonucleoside. Am. J. Physiol. Endocrinol. Metab. *288*, E980–E988.

Rodda, S.J., and McMahon, A.P. (2006). Distinct roles for Hedgehog and canonical Wnt signaling in specification, differentiation and maintenance of osteoblast progenitors. Development *133*, 3231–3244.

Takarada, T., Hinoi, E., Nakazato, R., Ochi, H., Xu, C., Tsuchikane, A., Takeda, S., Karsenty, G., Abe, T., Kiyonari, H., and Yoneda, Y. (2013). An analysis of skeletal development in osteoblast-specific and chondrocyte-specific runt-related transcription factor-2 (Runx2) knockout mice. J. Bone Miner. Res. *28*, 2064–2069.

Takeda, S., Bonnamy, J.P., Owen, M.J., Ducy, P., and Karsenty, G. (2001). Continuous expression of Cbfa1 in nonhypertrophic chondrocytes uncovers its ability to induce hypertrophic chondrocyte differentiation and partially rescues Cbfa1-deficient mice. Genes Dev. *15*, 467–481.

Tessa, A., Salvi, S., Casali, C., Garavelli, L., Digilio, M.C., Dotti, M.T., Di Giandomenico, S., Valoppi, M., Grieco, G.S., Comanducci, G., et al. (2003). Six novel mutations of the RUNX2 gene in Italian patients with cleidocranial dysplasia. Hum. Mutat. *22*, 104.

Vuorio, E., and de Crombrugghe, B. (1990). The family of collagen genes. Annu. Rev. Biochem. *59*, 837–872.

Wei, J., Hanna, T., Suda, N., Karsenty, G., and Ducy, P. (2014). Osteocalcin promotes β-cell proliferation during development and adulthood through Gprc6a. Diabetes *63*, 1021–1031.

Wilson, W.A., Hawley, S.A., and Hardie, D.G. (1996). Glucose repression/derepression in budding yeast: SNF1 protein kinase is activated by phosphorylation under derepressing conditions, and this correlates with a high AMP:ATP ratio. Curr. Biol. *6*, 1426–1434.

Woods, A., Munday, M.R., Scott, J., Yang, X., Carlson, M., and Carling, D. (1994). Yeast SNF1 is functionally related to mammalian AMP-activated protein kinase and regulates acetyl-CoA carboxylase in vivo. J. Biol. Chem. *269*, 19509–19515.

Yamashita, H., Takenoshita, M., Sakurai, M., Bruick, R.K., Henzel, W.J., Shillinglaw, W., Arnot, D., and Uyeda, K. (2001). A glucose-responsive transcription factor that regulates carbohydrate metabolism in the liver. Proc. Natl. Acad. Sci. USA *98*, 9116–9121.

Yu, K., Xu, J., Liu, Z., Sosic, D., Shao, J., Olson, E.N., Towler, D.A., and Ornitz, D.M. (2003). Conditional inactivation of FGF receptor 2 reveals an essential role for FGF signaling in the regulation of osteoblast function and bone growth. Development *130*, 3063–3074.

Zhang, M., Xuan, S., Bouxsein, M.L., von Stechow, D., Akeno, N., Faugere, M.C., Malluche, H., Zhao, G., Rosen, C.J., Efstratiadis, A., and Clemens, T.L. (2002). Osteoblast-specific knockout of the insulin-like growth factor (IGF) receptor gene reveals an essential role of IGF signaling in bone matrix mineralization. J. Biol. Chem. *277*, 44005–44012.

Zhao, M., Qiao, M., Oyajobi, B.O., Mundy, G.R., and Chen, D. (2003). E3 ubiquitin ligase Smurf1 mediates core-binding factor alpha1/Runx2 degradation and plays a specific role in osteoblast differentiation. J. Biol. Chem. *278*, 27939–27944.